



Article

# Effect of Heat Treatment on the Mechanical and Tribological Properties of Dual-Reinforced Cold-Sprayed Al Coatings

Kia Min Phua <sup>1</sup>, Thomas Stapel <sup>2</sup> and Troy Y. Ansell <sup>1,\*</sup>

<sup>1</sup> Coatings and Composites for Extreme Environments Lab (CE)<sup>2</sup>, Department of Mechanical and Aerospace Engineering, Naval Postgraduate School, Monterey, CA 93943, USA

<sup>2</sup> NanoMEMS Laboratory, Department of Physics, Naval Postgraduate School, Monterey, CA 93943, USA

\* Correspondence: troy.ansell@nps.edu

**Abstract:** The aluminum cold spray feedstock powder was single- and dual-reinforced with no greater than 2 vol% boron nitride nanoplatelets (BNNP) and/or nanometric boron carbide (nB<sub>4</sub>C). These powders were cold sprayed onto Al-6061 substrates and then heat-treated in an argon environment. In addition, micro- and nano-indentation hardness and wear testing were performed on the heat-treated samples. Further microscopy and optical profilometry were used to characterize the microstructure and wear track volumes. Minimal changes to the splat structure were observed after heat treatment. However, when compared to the pure Al coating, microhardness improved with reinforcement after treatment at 500 °C, while nanohardness improved only in the dual-reinforced coatings, again after treatment at 500 °C. The elastic modulus generally decreased for the reinforced coatings after treatment; however, indentation test results were mixed. The wear testing done on samples heat treated at 500 °C for one hour showed increases in the specific wear rate for single-reinforced coatings but decreases in the dual-reinforced coatings. These results indicate that both dual-reinforcement and heat treatment are required for improvements in the mechanical and tribological properties of Al nanocomposites.

**Keywords:** cold spray; boron nitride nanoplatelets; aluminum metal matrix composites; dual-reinforced coatings



**Citation:** Phua, K.M.; Stapel, T.; Ansell, T.Y. Effect of Heat Treatment on the Mechanical and Tribological Properties of Dual-Reinforced Cold-Sprayed Al Coatings. *J. Manuf. Mater. Process.* **2023**, *7*, 32. <https://doi.org/10.3390/jmmp7010032>

Academic Editors: Olexandr Grydin and Florian Nürnberger

Received: 15 December 2022

Revised: 14 January 2023

Accepted: 23 January 2023

Published: 28 January 2023



**Copyright:** © 2023 by the authors. Licensee MDPI, Basel, Switzerland. This article is an open access article distributed under the terms and conditions of the Creative Commons Attribution (CC BY) license (<https://creativecommons.org/licenses/by/4.0/>).

## 1. Introduction

The cold gas dynamic spray, or “cold spray”, is a thermal spray technique and an additive manufacturing technology used primarily for the application of metal and metal-ceramic coatings but is also gaining traction for use in metal component repair [1,2]. However, unlike other thermal spray techniques, such as plasma spray, cold spray does not require the melting of the feedstock powder prior to spraying. Instead, deposition and adhesion result from the high kinetic energy of the feedstock powders upon contact with a substrate. The adhesion is possible through a combination of two mechanisms: mechanical interlocking and metallic bonding [3,4]. This gives cold spray some advantages over other thermal spray techniques, such as the avoidance of high temperature oxidation and deleterious secondary phase reactions; lower residual stresses, which could lead to relatively thicker coatings; and lower barriers to portability [2,3,5]. The last advantage is especially critical for the in-situ repair of seagoing vessels and deployed equipment, making cold spray desirable to the industry and militaries looking to limit disruptions to supply chains and reduce deployment costs [6,7].

The alloys of Al possess excellent strength-to-weight ratios, making them desirable for applications where weight is a concern, such as in aircraft. Future applications, however, will demand greater strength and wear resistance in structural and component materials. Al metal matrix composites (MMC) are increasingly being looked at to improve the strength and wear resistance of Al without sacrificing its ductility, corrosion resistance, etc. [8,9]. The

Al-MMCs are being utilized in both the aerospace and automotive industries for their high specific strength [10,11], high specific stiffness [12], and good wear resistance [13–15]. As a result of the advantages of cold spray, there is growing interest in cold spray Al MMC. In addition, cold sprayed Al MMC coatings have shown improvements in the mechanical and tribological properties over base Al cold sprayed coatings; however, poor tensile strength limits their application [16].

Heat treatment is often employed to change the grain size and improve the mechanical properties of metallic materials. The same has been shown to be true for cold-sprayed coatings. Huang et al. and Rokni et al. separately showed improvements in the mechanical properties of Al cold-sprayed coatings after annealing [17,18]. Rokni et al. showed that for Al-7075, annealing above 370 °C increased the coating hardness due to recrystallization of the elongated cold spray grain structure to an equiaxed grain structure [18]. In another similar study on cold-sprayed Al-6061, Rokni et al. showed recrystallization was responsible for increases in coating hardness near splat boundaries [19]. The heat treatment alone, however, will not improve both mechanical properties and wear resistance. Loganathan et al. looked at the combined effects of reinforcement (nano-diamond) and heat-treatment of a cold-sprayed Al coating [20]. They found the presence of nanodiamond inhibited grain growth but improved hardness and the wear rate after heat treatment. In order to improve both the mechanical properties and wear resistance of Al MMCs that are cold sprayed, Al MMC coatings will be reinforced with two particles, sprayed onto an Al substrate, and then coated samples will be heat treated. It is the aim of this paper to show the synergistic effects of both dual-reinforcement and heat treatment on the properties of Al-MMCs.

## 2. Materials and Methods

### 2.1. Sample Preparation

The powders were processed following the same procedures as a previous study [21]. The matrix phase was composed of 99.5% Al (SST5001; Centerline Limited; Windsor, ON, Canada). The reinforcing phases included nanometric boron carbide ( $nB_4C$ ) with >99% purity (US2140; US Research Nanomaterials Inc.; Houston, TX, USA) and boron nitride nanoplatelets (BNNP, 1523DX; SkySpring Nanomaterials; Houston, TX, USA). The coatings were sprayed onto plates of Al 6061, which were grit-blasted prior to spraying. The coating compositions were the same as those studied by Norrell et al. and sprayed under the same conditions [21]. A schematic of the compositions is shown in Figure 1. Compositions A1 through A4 correspond to compositions “A”, “A-C”, “A-N”, and “A-CN”, respectively, from the work of Norell et al. Compositions A2, A3, and A4 were cryomilled (five cycles of two minutes on and two minutes off each). To form composition A5, powder was taken from both A2 and A3 and further mixed in a high-energy ball mill (SPEX-8000; SPEX SamplePrep, LLC; Metuchen, NJ, USA) without milling media.

Each composition set was split into five samples. One sample was left untreated as a control, while the other four samples were subjected to four annealing conditions. Prior to heat treatment, cross-sections were cut from each sample to expose the coating and substrate. A heat treatment was carried out in a 0.03 MPa Ar environment contained within a clamshell furnace (OTF-1200X; MTI Corporation; Richmond, CA, USA). In addition, the samples were heated to the annealing temperature at a rate of 5 °C/min and held for 1 or 4 h. The samples were then furnace-cooled to room temperature. The different heat treatment conditions are listed in Table 1. In order to keep track of compositions treated under these conditions, the sample nomenclature will include the composition (A1, A2, etc.) and the treatment condition (C1, C2, etc.). The composition and condition will be separated by an underscore, e.g., the coating reinforced with BNNPs and heat-treated at 300 °C for four hours will be labeled A2\_C3.

### 2.2. Sample Characterization

Both the as-sprayed and heat-treated samples were encased in a thermolytic epoxy (DuroFast; Struers; Copenhagen, Denmark) using a hot mounting press (CitoPress; Struers).

A coarse and fine grinding were performed using 320, 800, and 1200-grit SiC paper. The coarse polishing was carried out on a polishing cloth with a 3 and 1  $\mu\text{m}$  monocrystalline diamond suspension, followed by fine polishing with a 0.06  $\mu\text{m}$  colloidal  $\text{SiO}_2$  suspension. The polished samples were then etched using Keller’s reagent (1 mol% HF, 1.5 mol% HCl, 2.5 mol%  $\text{HNO}_3$ , balance  $\text{H}_2\text{O}$ ) for 30 s. An optical metallography was performed on the samples using an inverted optical microscope (Epiphot 200; Nikon; Japan).

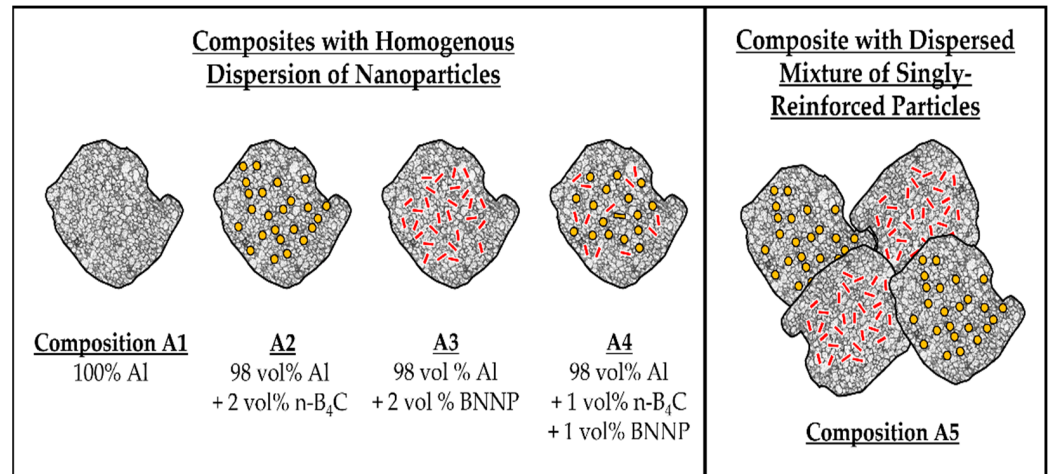


**Figure 1.** Schematic of compositions. Nanometric  $\text{B}_4\text{C}$  represented by yellow dots and the red bars represent the BNNTs. Composition A4 will also be referred to as the homogeneous dual-reinforced coating. Composition A5 will also be referred to as the dispersed dual-reinforced coating.

**Table 1.** Temperature and holding time of heat-treatment conditions labeled as C1, C2, etc. This nomenclature will be used for the rest of the paper to identify the sample.

C1	C2	C3	C4	C5
As-sprayed	Annealed at 300 °C for 1 h	Annealed at 300 °C for 4 h	Annealed at 500 °C for 1 h	Annealed at 500 °C for 4 h

Additionally, a microhardness test on the Vicker’s scale was performed on a micro-indenter (DuraScan; Struers; Copenhagen, Denmark) with a maximum load of 50 g held for 10 s. Arrays of 15 indentations (3 rows of 5 indentations) were made with 30  $\mu\text{m}$  spacing between points. A nanoindentation was performed in a nano-indenter tester (G200; Agilent Technologies; Santa Clara, CA, USA) with a maximum load of 29.42 mN, which was held for 3 s. An array of 50 Berkovich indentations (5 rows of 10 indentations) was made with 20  $\mu\text{m}$  spacing between indents. This was done to obtain the hardness and modulus via the Oliver-Pharr method [22]. Additionally, the work of indentation (WOI) was obtained by calculating the area under the load-displacement curves [23,24]. The trapezoidal rule of integration was used for these calculations in Matlab, which has a built-in function for this purpose.

A T50 tribometer (Nanovea, Irvine, CA, USA) was used to conduct ball-on-disk abrasive wear testing. A 25.4 mm  $\times$  25.4 mm coated sample of each composition heat-treated with condition 4 (C4) was wear-tested. A 5.0 N normal load was applied to the coated surface with a 3.0 mm diameter alumina contact ball in dry conditions. The wear track diameter was 3.0 mm, and the wear test was conducted at 100 RPM for 30 min. For each sample, 5 wear tests were completed, and the mass loss and average coefficient of friction (COF) were recorded. The wear debris was collected after each test for further analysis in a Neon 40 scanning electron microscope (SEM; Zeiss; Oberkochen, Germany). A SEM imaging experiment was conducted with an accelerating voltage of 20 kV at a working distance of 5 mm and an objective aperture of 60  $\mu\text{m}$ . The average wear debris size was

determined by using Feret's diameter, where the most significant distance between two points of the debris particle was recorded. An image processing software, ImageJ, was used to analyze the distribution of the particle sizes of the wear debris collected.

Furthermore, a depth profile was performed to characterize the volume of the wear tracks. Using an optical profilometer (NewView 7100; Zygo; Middlefield, CT, USA), ten optical profiles were generated per wear track. The average wear depth as a function of wear track width, estimated profile area, and profile volume were measured for each profile. In turn, the profile was used to approximate the wear volume and calculate the average density of the coating. The volume of each track was approximated by calculating the cross-sectional area of a halved ellipse multiplied by  $2\pi \times 1.5$  mm. The specific wear rate was calculated using the normal load of 5 N and the travel distance of the wear ball, which was 28.260 m.

### 3. Results

#### 3.1. Splat Structure

Optical micrographs seen in Figure 2 are of the coating-substrate interface for compositions A1\_C4 (Figure 2a) and A5\_C4 (Figure 2b). A lower magnification optical images for all samples can be seen in Figure A1. In general, the splat structures for all as-sprayed compositions were similar. In addition, inter-splat grain bridging and growth were not observed after heat treatment, as was also seen by the investigation of Hall et al. [25]. Although in that case the Al coatings were annealed for 22 h at 300 °C, the samples in this work were treated for only one to four hours. However, grain growth across splat boundaries was not observed at any temperature or annealing time. Although grain structure was not investigated with electron backscatter diffraction in this work, because the cold sprayed coatings were primarily Al and the reinforcing particles reside at the splat boundaries, changes to grain structure, i.e., recrystallization, would occur within a splat similar to that observed by Rokni et al. and Hall et al. [18,18,25], an example of possible recrystallization can be seen in Figure A2 for A1\_C4.

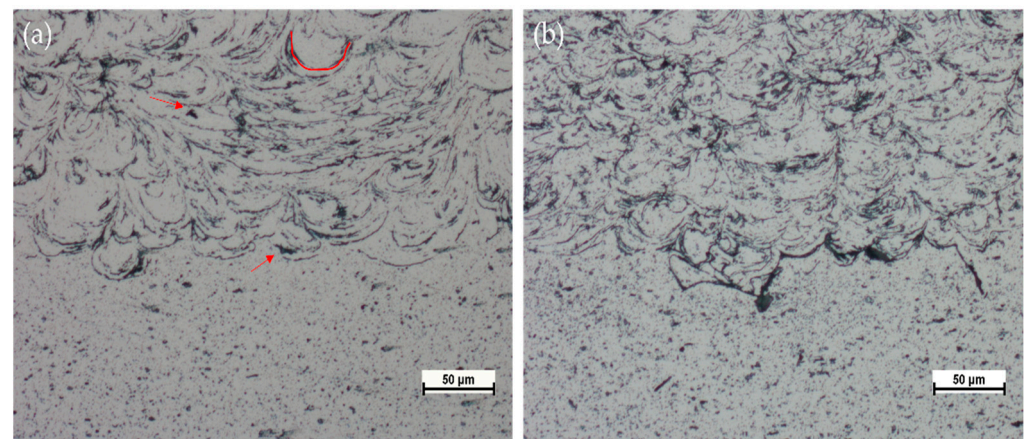


**Figure 2.** Optical images of compositions A1\_C4 in (a) and A5\_C4 in (b). Red arrows indicate examples of pores in the coating and at the interface. A representative splat boundary is indicated by the solid red line.

#### 3.2. Mechanical Properties

The mean results of micro-indentation tests for each composition and their corresponding heat treatments are shown in Figure 3. Except in one case, micro-indentation hardness was higher in the composite coatings versus A1\_C1. The hardness drops as the annealing temperature increases but keeps relatively constant when annealing times increase from one to four hours. This can be attributed to changes in grain size (i.e., recrystallization) of the Al matrix. In addition, from the changes in microhardness with heat treatment and the lack of any significant difference in hardness between the control and reinforced samples, it can

be inferred that mechanical changes in the Al matrix are dominating any hardening effects from the reinforcements. The evaluation of images of the indents revealed brittle features in the control samples that changed to ripple-like features after heat treatment, indicative of plastic deformation. This indicated more plastic deformation after heat treatment.

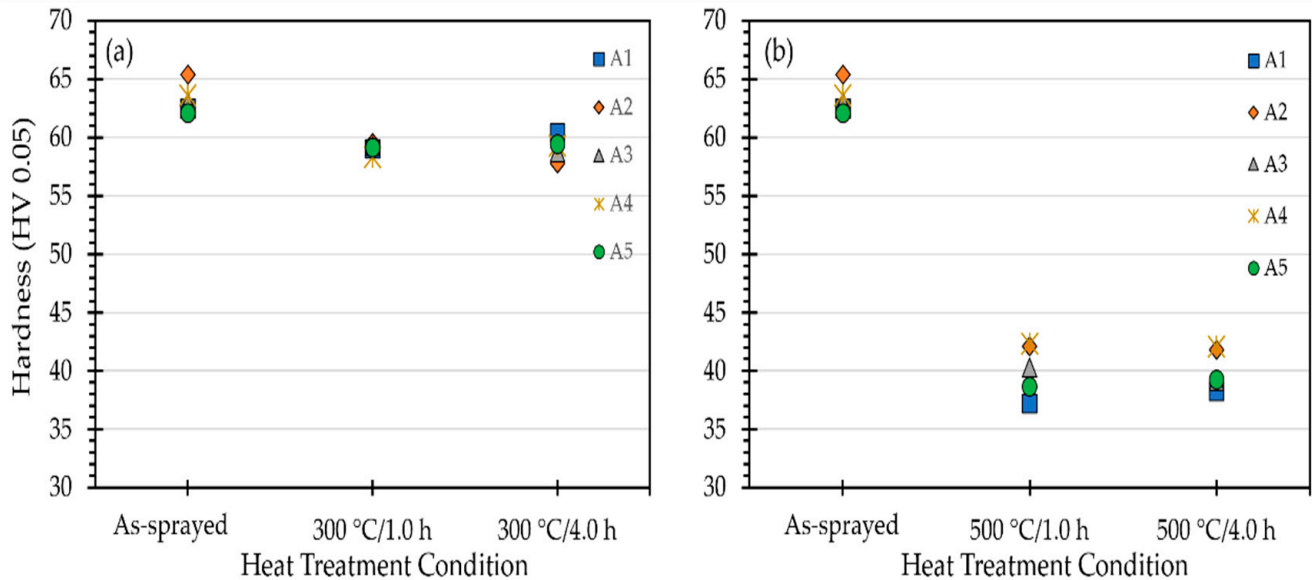
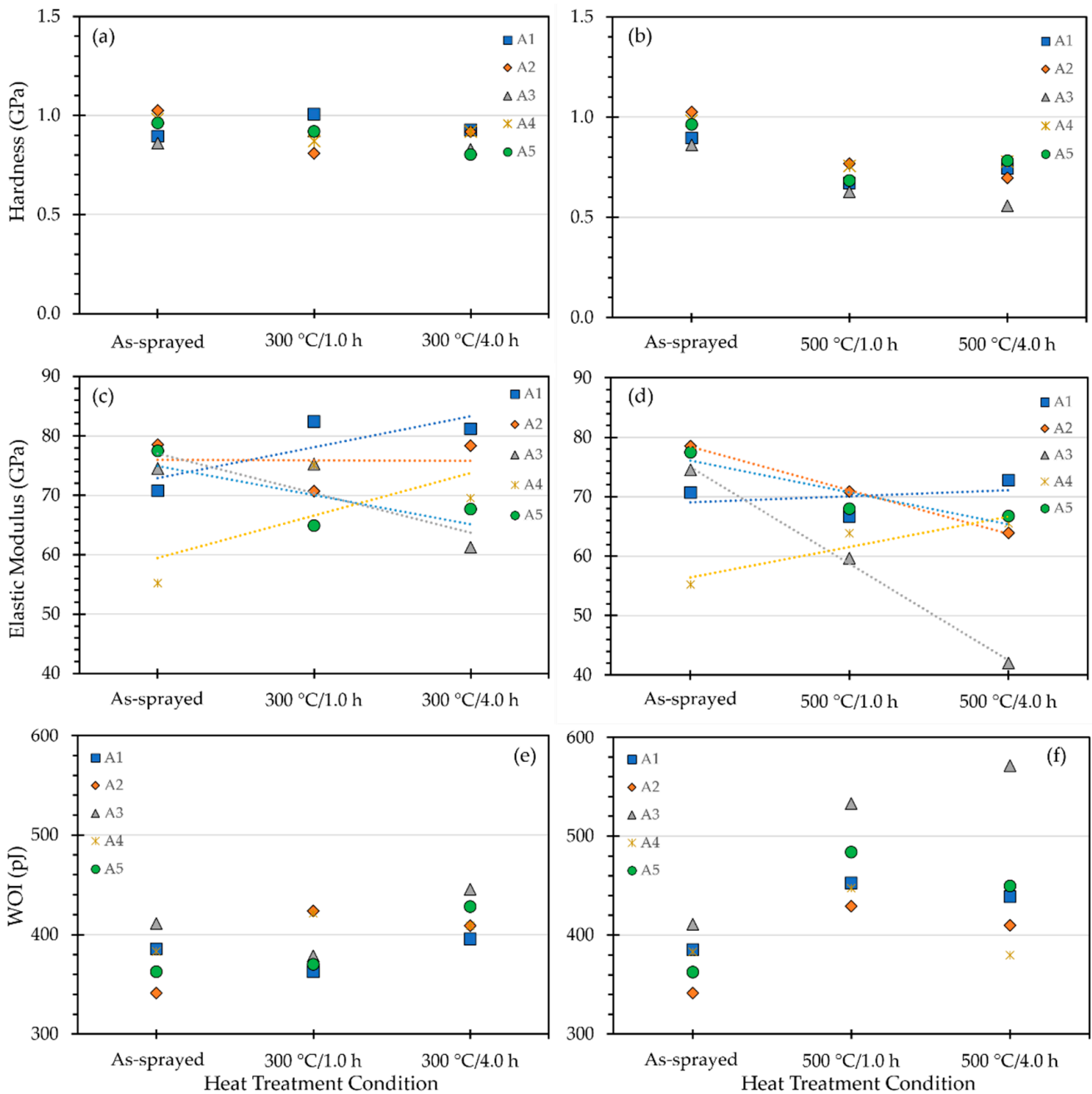


**Figure 3.** Results from microindentation tests. Samples treated at 300 °C shown in (a) while those treated at 500 °C in (b). The control is the as-sprayed or as-received sample.

Furthermore, nanoindentations were performed for each composition and its corresponding heat treatments. Assuming the data is normally distributed, the Grubbs' test was used to iteratively remove outliers from the nanoindentation data [26,27]. The resulting hardness, elastic modulus, and work of indentation (WOI) were then averaged and plotted in Figure 4. In observing the nano-indentation hardness (Figure 4a,b), the value decreased when the annealing temperature was 300 °C, with no further change observed with an increase in the annealing duration. A downward trend was observed in all four reinforced compositions (A2–A5) with an annealing temperature of 500 °C. Elastic modulus (Figure 4c,d) exhibited more scatter than hardness; however, a general trend observed was a decrease in modulus for most compositions after annealing.

Figure 4e,f show the WOI of the samples. Composition A3\_C1 exhibited the highest plasticity of the as-sprayed samples; a 300 °C treatment leads to small changes in WOI at this temperature. A comparison of Figure 4c–f shows this inverse dependence for each composition. The results from Figure 4 also match those seen in Figure 3. Despite the contradictory results seen in micro- and nano-indentation hardness data, when modulus and WOI results are considered, a clearer story is resolved. The differences seen in the indentation hardness data are due to the different length scales. Micro-indentation images, however, revealed increases in local ductility in annealed samples. Additionally, elastic modulus and WOI show small-scale improvements to the plasticity of the annealed coatings.

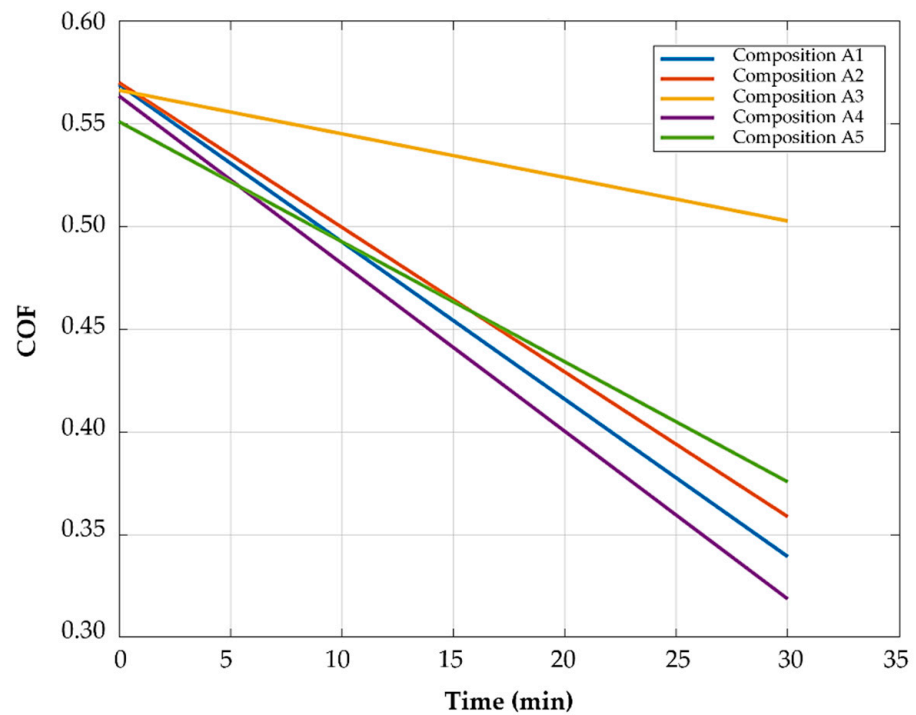
The indentation testing showed improvements in the mechanical properties of samples, especially those that underwent C4 treatment. This is confirmed when considering results from the WOI, where C4 samples showed between 16 and 30% improvement in compressive work when compared to the as-sprayed samples. Therefore, these samples, heat-treated with the C4 treatment, were chosen to undergo wear testing to study the tribological properties of the annealed reinforced coatings.



**Figure 4.** Nano-indentation hardness comparing (a), control to 300 °C for 1 h or 4 h, or (b), 500 °C for 1 h or 4 h. Elastic modulus (c), at 300 °C for 1 h or 4 h or (d), 500 °C for 1 h or 4 h. WOI, (e), at 300 °C for 1 h or 4 h or (f), 500 °C for 1 h or 4 h.

### 3.3. Tribological Properties

The least-squares fits of the COF as a function of time are plotted in Figure 5 for all five compositions annealed with Condition 4. An example of the fitting of COF with time can be found in the Appendix A (Figure A3). From Figure 5, it is seen that composition A4\_C4 had the lowest COF vs. time as compared to the other compositions for most of the wear tests. Composition A3\_C4 had a relatively stable, albeit high, COF during wear testing. The single or dual reinforced coatings, however, with nB<sub>4</sub>C showed a reduced COF over time. The composition A5\_C4, with distinct nB<sub>4</sub>C / BNNP rich regions, showed a less steep decrease in COF as compared to the Al-MMCs added with nB<sub>4</sub>C. It can be deduced that adding nB<sub>4</sub>C reduces the coating COF while adding BNNP stabilizes the COF of the Al-MMC coating under abrasive wear.



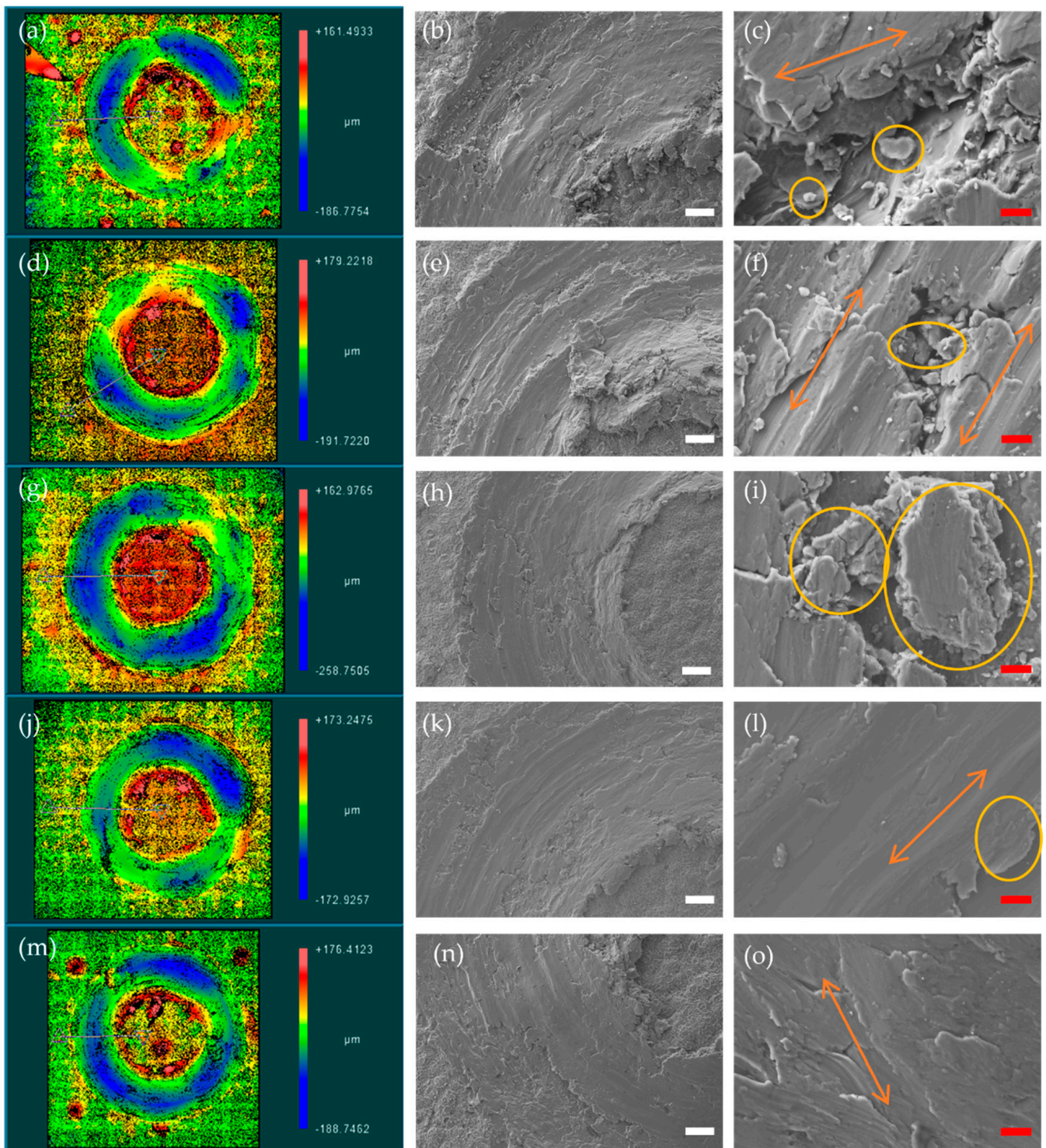
**Figure 5.** Average COF as a function of time for the five compositions annealed at 500 °C for one hour.

Figure 6 has optical profilometry images of the wear tracks from each C4 sample as well as low- and high-magnification SEM images of the same wear tracks. The control, A1\_C4, and the dispersed dual-reinforced sample, A5\_C4, had similar depths after wear. The deepest tracks were seen in the BNNT coating A3\_C4, while the shallowest was seen in the homogenous dual-reinforced coating, A4\_C4. SEM imaging revealed plough grooves, secondary cracking, and delaminated particles within the wear tracks of each coating. The delaminated particles heavily populated the wear tracks of compositions A1, A2, and A3, but were rarely found in either dual-reinforced coating. The groove marks seen in A3 appear deeper and finer than those found in A2. The composition in A4 exhibited less delamination and smoother wear tracks than A5.

Listed in Table 2 are the average COF, average mass loss, and the specific wear rate of the five samples heat treated under the C4 condition. The average COF was the same for all five samples. The pure Al coated sample, A1\_C4, saw the lowest amount of mass loss after wear testing. In comparison, the single-reinforced BNNT composition, A3\_C4, lost the most mass. Sample A2\_C4 along with the dual-reinforced A4\_C4 and A5\_C4 samples, experienced similar mass losses. In comparing the dual-reinforced samples, A5\_C4 showed greater mass loss than A4\_C4, which is linked to the distinct nB<sub>4</sub>C and BNNT regions in A5\_C4. Further, adding nB<sub>4</sub>C to the MMC coating helps control the amount of mass loss, while adding BNNT appears to result in greater mass loss. Specific wear rates saw increases with the single-reinforced coatings, while the dual-reinforced coatings had similar rates when compared to A1.

**Table 2.** Coefficient of friction (COF), mass loss, and specific wear rate of samples A1–A5 heat-treated with condition 4 (C4).

	A1	A2	A3	A4	A5
COF	0.48	0.47	0.51	0.46	0.48
Mass Loss (mg)	1.24	1.54	2.54	1.50	1.56
Specific Wear Rate (mm <sup>3</sup> /Nm)	0.00405	0.00580	0.00596	0.00391	0.00417



**Figure 6.** Depth profiles (left-hand column) and SEM images (40–50X in the middle column and 500X in the right-hand column) of five compositions annealed at 500 °C for one hour (condition 4 or C4) composition A1\_C4 in (a–c), A2\_C4 in (d–f), A3\_C4 in (g–i), A4\_C4 in (j–l), and A5\_C4 in (m–o). White scale bar in lower magnification SEM images corresponds to 50 μm. Red scale bar in 500X SEM images is 10 μm. Ploughing grooves represented by orange double arrows. Fully or partially delaminated particles indicated by yellow circles.

The wear debris was analyzed in the SEM. The average wear size for each C4 sample is listed in Table 3. The debris, i.e., the delaminated particles, had a flattened morphology with rough edges. Adding nB<sub>4</sub>C to the Al-MMC coating created smaller wear debris. This

may indicate a coating that is slightly more brittle and/or less cohesive than the other coating compositions. Adding BNNP to the composite resulted in larger debris (the largest among the reinforced coatings). In A4, adding BNNP resulted in debris sizes similar to A3. The composition in A5 produced large average wear debris compared to the other compositions annealed with condition 4.

**Table 3.** Average wear debris size, standard deviation, and maximum and minimum observed debris sizes for each of the compositions that underwent wear testing.

	A1_C4	A2_C4	A3_C4	A4_C4	A5_C4
Average Wear Debris Size ( $\mu\text{m}$ )	107	49.5	78.7	68.9	138
$\sigma$ ( $\mu\text{m}$ )	118	69.7	98.3	99.7	109
Max ( $\mu\text{m}$ )	1128	840	994	1202	669
Min ( $\mu\text{m}$ )	7.03	6.39	6.50	6.73	13.6

## 4. Discussion

### 4.1. Discussion of Hardness Results

The reinforcement of the as-sprayed coatings saw no changes in microhardness but increases in nanohardness of up to 15%. In addition, reinforcement of the coatings saw either no change or decreases in hardness at both scales when annealed at 300 °C. At 500 °C, however, the reverse was true, with increases in microhardness of up to 14% and 15% in nanohardness. The previous comparisons were made between A1 samples with the same treatment condition. Further, comparisons are made between the same compositions as-sprayed and annealed. The annealing at 300 °C for one hour led to decreases in microhardness of between 5 and 9%, and for four hours, between 3 and 12%. When the temperature was 500 °C, the decrease was between 33 and 40%, regardless of time. For nanohardness, the changes were much more scattered but generally less than those seen in microhardness.

The smaller and often scattered changes in nanohardness are due to the location of the nanoparticles after spraying and the small size of the indenter. However, nano-indentation testing is more localized than micro-indentation hardness testing because the indents likely fall within a splat instead of including splat boundaries in the measurement where BNNPs and  $\text{nB}_4\text{C}$  reside. This explains the differences between micro- and nano-hardness changes. Further, dual reinforcement of the Al did clearly lead to increases of up to 15% in hardness at both scales and across both annealing temperatures.

The elastic modulus was “noisier,” but one trend that could be gleaned from the data is that A1 exhibits a lower modulus compared to the composite coatings as-sprayed, but after annealing, exhibited a higher modulus with some exceptions. In addition, the elastic modulus decreased for compositions C2, C3, and BNNPs, which, experienced larger decreases in modulus, especially after annealing at 500 °C. The homogenous, dual-reinforced coating saw increases in stiffness with annealing. Adding  $\text{nB}_4\text{C}$  had a stiffening effect, while adding BNNPs softened the Al composite. The highest improvements in WOI performance of the Al-MMC were observed with BNNP composites. Both A3 and A5 saw improvements in their WOI performance as the annealing temperature and time were increased. The addition of  $\text{nB}_4\text{C}$  led to improvements in WOI only with condition 2 treatment; however, longer anneal times and/or higher anneal temperatures resulted in a minimal improvement in WOI.

### 4.2. Discussion of Wear Results

The addition of  $\text{nB}_4\text{C}$  or BNNP had little effect on the COF but had a measurable and adverse effect on the specific wear rate. The  $\text{nB}_4\text{C}$  or BNNP anchored adjacent splats. When one splat came out during wear testing, the attached splat had a higher probability of also detaching from the coating. Interestingly, the wear debris size was smaller in the mean and in the size distribution for both A2\_C4 and A3\_C4 when compared to A1\_C4.

This contributed to the increase in mass loss and subsequent reduction in wear rate of the single-reinforced coatings. It should be noted that the splats in the A1\_C4 coating were more elongated as compared to the more equiaxed splat structures observed in both A2\_C4 and A3\_C4 (refer to Figure A1). Unlike the single-reinforced compositions, similar specific wear rates and COF were measured for the dispersed, distributed dual-reinforced coating annealed with condition 4 (A5\_C4). On average, the wear debris was larger for this composition as compared to the A1\_C4 composition; however, the size distribution was almost half that observed in A1, and the largest piece of debris imaged was nearly half the width of that observed in A1\_C4. The homogeneous dual-reinforced sample (A4\_C4) experienced a reduction in COF and specific wear rate and produced smaller average wear debris.

The harder  $nB_4C$  likely caused the deepest, smallest cuts in the wear grooves seen in Figure 6. To a lesser extent than seen in A2\_C4, BNNPs in A3\_C4 also caused deep and small cuts within wear grooves. In a study by Paul et al., variations in hardness in hexagonal boron nitride (hBN)-reinforced cast aluminum were due to the random orientation of the 2D plate-like hBN that could be perpendicular or parallel to the indentation load [28]. Similarly, the orientation of BNNPs, e.g., angled or perpendicular to splat surfaces, resulted in a higher COF. The BNNPs that were oriented parallel to the wear surface, however, acted as a lubricative phase and could have led to the low reduction in COF over time. Despite acting as anchors between splats and between splats and the substrate, both nanoparticles contributed to the increased wear rates of their respective compositions. A suggested schematic for this is shown in Figure 7a for A3\_C4 with BNNPs. During wear tests, the delaminated splats with attached nanoparticles acted as third-party wear particles, causing more abrasion of the coating.

Conversely, both dual-reinforced samples saw reduced or similar wear rates compared to the baseline. When the two nanoparticles are homogeneously dispersed across the splats, there is less surface area covered by the harder particles. So, when a splat delaminates from the coating, there is a smaller chance for a  $nB_4C$  particle or an angled BNNP to attach itself to a splat still connected to the coating. A schematic for the tribology of A5\_C4 is shown in Figure 7b. The larger wear debris collected from A5\_C4 could be attributed to the additional processing step A5 samples underwent. While A4\_C4 underwent cryomilling just as compositions A1–A3, samples of cryomilled A2 and A3 powders were further mixed together in a high-energy ball mill to produce A5 [21]. This additional mixing led to larger, flatter composite particles, which in turn led to the larger splats of the A5 samples seen in Figure A1.

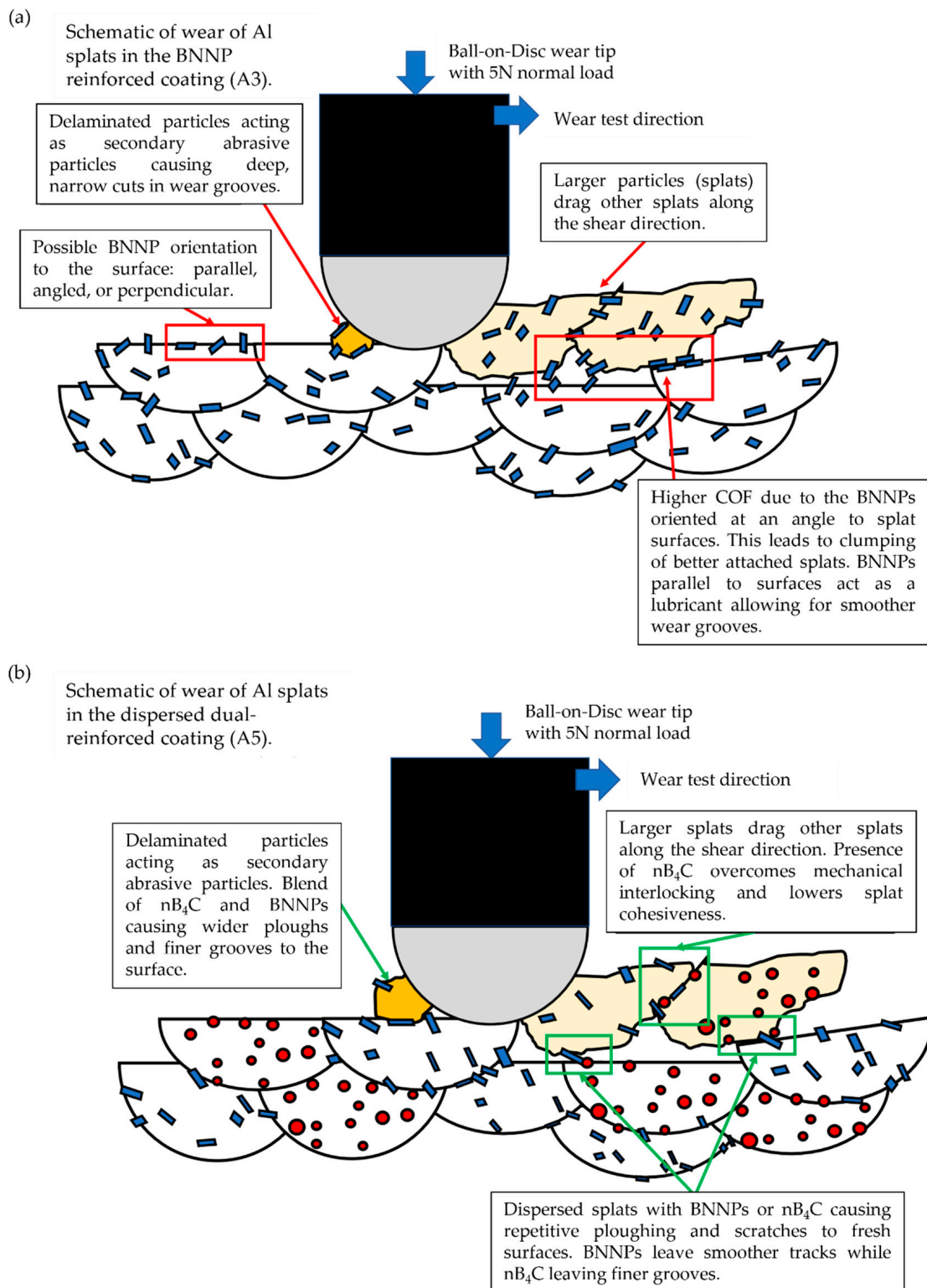


**Figure 7.** Illustrations of the pin-on-disk wear tip ploughing across the surface of composite coatings. Representation of (a) A3\_C4 and (b) A5\_C4.

### 5. Conclusions

In this study, two nanoparticles,  $nB_4C$  and BNNP, were incorporated into Al feedstock powders and cold sprayed onto an Al-6061 substrate. The heat treatment of the composites led to a characteristic softening of the samples, indicating that recrystallization effects dominated changes in mechanical properties over the reinforcing effects of the nanoparti-

cles. In addition, single reinforcement and heat treatment led to deleterious increases in wear rate compared to the pure Al-coated sample. The homogeneous dual reinforcement, however, led to slight improvements in the specific wear rate after annealing at 500 °C. This reinforcement was the result of cryomilling Al powders with both nanoparticles as opposed to cryomilling Al with  $nB_4C$  or BNNP separately and then using a HEBM for a final mixing. The manner in which the nanoparticles are distributed affects the properties, while in homogeneous dual-reinforcement, the two appear to cooperatively improve the wear properties.

**Author Contributions:** Conceptualization, K.M.P.; methodology, K.M.P.; validation, K.M.P. and T.Y.A.; formal analysis, K.M.P., T.S. and T.Y.A.; investigation, K.M.P., T.S. and T.Y.A.; resources, T.Y.A.; data curation, K.M.P.; writing—original draft preparation, T.Y.A.; writing—review and editing, K.M.P. and T.Y.A.; visualization, K.M.P. and T.Y.A.; supervision, T.Y.A.; project administration, T.Y.A. All authors have read and agreed to the published version of the manuscript.

**Funding:** This research was funded, in part, by the Office of Naval Research, grant number N0001422WX00041.

**Data Availability Statement:** Not applicable.

**Acknowledgments:** The authors would like to acknowledge Gehn Ferguson and Aaron Nardi of the US Army Research Lab, who sprayed the substrates. We would also like to thank Travis Norrell for selecting the compositions and laying the baseline for our study. Finally, we would like to dedicate this work to the memory of Andy Nieto. This work would not have been possible without his vision for metal matrix nanocomposites and cold spray and his passion for materials science. He passed on too soon; he will be greatly missed.

**Conflicts of Interest:** The authors declare no conflict of interest.

## Appendix A

Figure A1 showcases optical micrographs for all samples investigated in this work, taken with a 10X objective lens. All images correspond to the sample coating-substrate interface and are representative of that sample interface. Figure A2 shows possible recrystallization after heat treatment of A1\_C4. Figure A3 shows an example of the real COF data (A3\_C4 in this case) and how it was fitted to each C4 sample that underwent wear testing. Figure 5 was assembled from this fitted data.

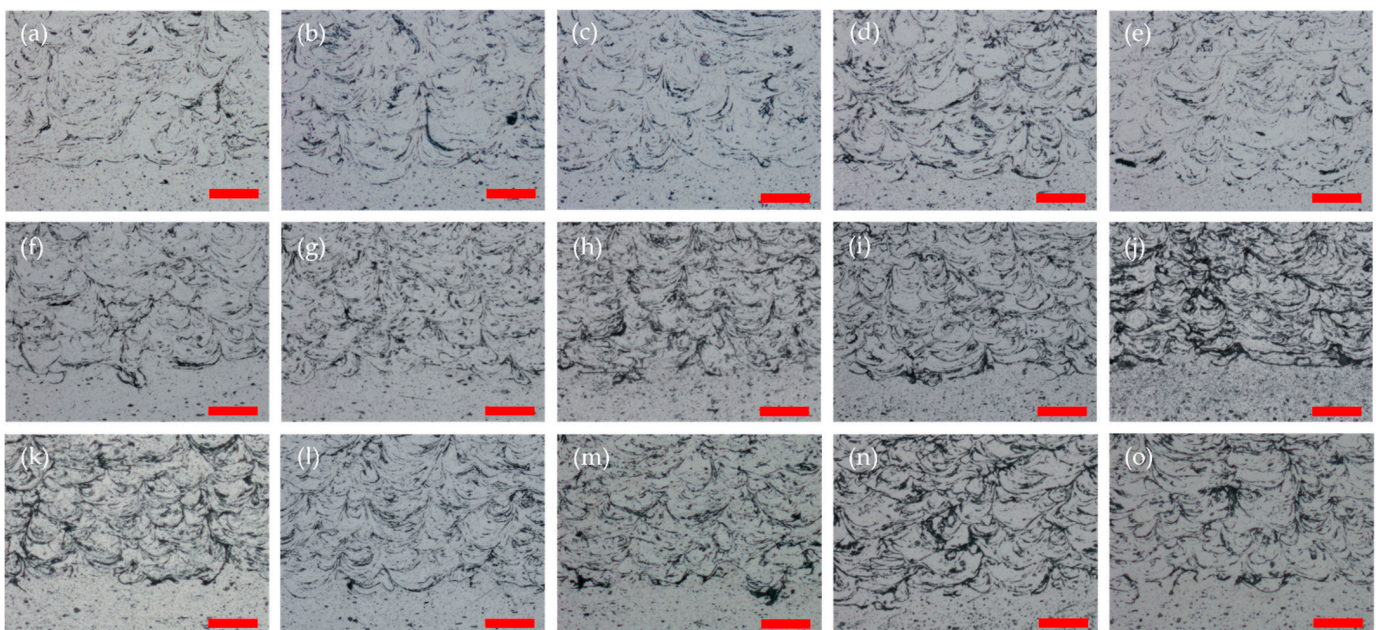
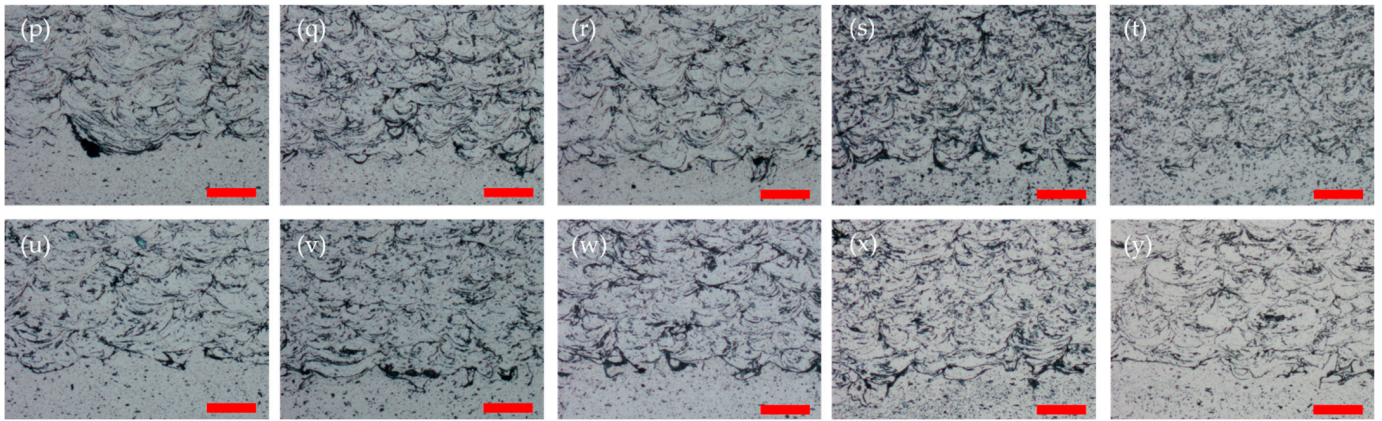
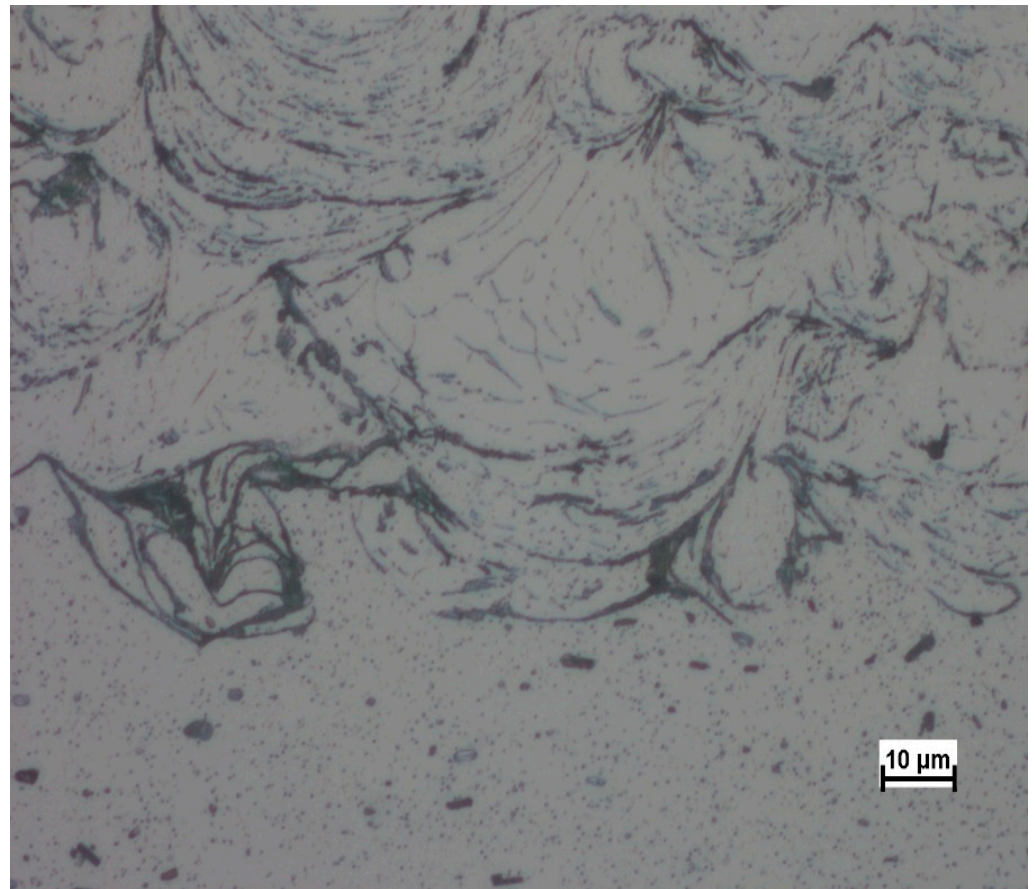


Figure A1. Cont.



**Figure A1.** Optical images of all samples after spraying and/or heat treatment. Images in first row are of pure Al coating (composition A1), starting with the as-sprayed condition (C1) on the left and going to C5 on the right. The same for the other compositions. First row has compositions A1\_C1 in (a), A1\_C2 in (b), A1\_C3 in (c), A1\_C4 in (d), and A1\_C5 in (e). Second row has compositions A2\_C1 in (f), A2\_C2 in (g), A2\_C3 in (h), A2\_C4 in (i), and A2\_C5 in (j). Third row has compositions A3\_C1 in (k), A3\_C2 in (l), A3\_C3 in (m), A3\_C4 in (n), and A3\_C5 in (o). Fourth row has compositions A4\_C1 in (p), A4\_C2 in (q), A4\_C3 in (r), A4\_C4 in (s), and A4\_C5 in (t). Fifth and bottom row have compositions A5\_C1 in (u), A5\_C2 in (v), A5\_C3 in (w), A5\_C4 in (x), and A5\_C5 in (y). Scale bar is 50  $\mu\text{m}$ .



**Figure A2.** Higher magnification optical image of sample A1\_C4.

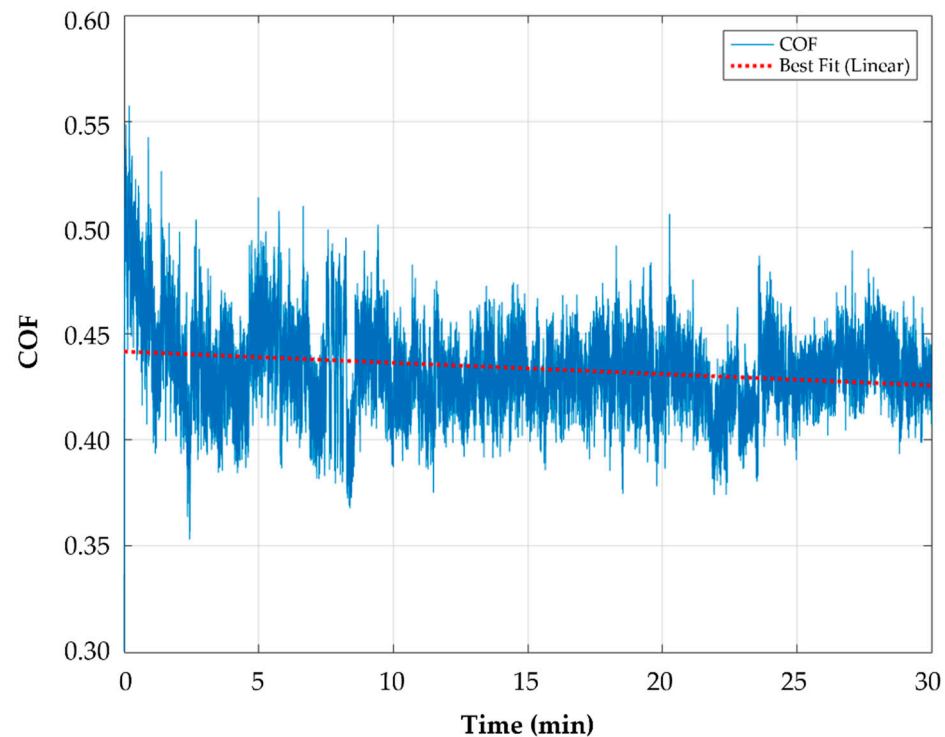


**Figure A3.** Example of the linear regression or least-squares fitting performed on the COF data of composition A3\_C4.

## References

1. Raelison, R.N.; Verdy, C.; Liao, H. Cold Gas Dynamic Spray Additive Manufacturing Today: Deposit Possibilities, Technological Solutions and Viable Applications. *Mater. Des.* **2017**, *133*, 266–287. [[CrossRef](#)]
2. Moridi, A.; Hassani-Gangaraj, S.M.; Guagliano, M.; Dao, M. Cold Spray Coating: Review of Material Systems and Future Perspectives. *Surf. Eng.* **2014**, *30*, 369–395. [[CrossRef](#)]
3. Hussain, T.; McCartney, D.G.; Shipway, P.H.; Zhang, D. Bonding Mechanisms in Cold Spraying: The Contributions of Metallurgical and Mechanical Components. *J. Therm. Spray Technol.* **2009**, *18*, 364–379. [[CrossRef](#)]
4. Champagne, V.K.; Helfrich, D.; Leyman, P.; Grendahl, S.; Klotz, B. Interface Material Mixing Formed by the Deposition of Copper on Aluminum by Means of the Cold Spray Process. *J. Therm. Spray Technol.* **2005**, *14*, 330–334. [[CrossRef](#)]
5. Champagne, V.K. The Repair of Magnesium Rotorcraft Components by Cold Spray. *J. Fail. Anal. Prev.* **2008**, *8*, 164–175. [[CrossRef](#)]
6. *Additive Manufacturing and Obsolescence Management in the Defence Context*; Rand Corporation: Santa Monica, CA, USA, 2015.
7. Hussein, T. US NAVSEA Develops Cold Spray Technique for Ship Maintenance. *Nav. Technol.* **2019**.
8. He, L.; Hassani, M. A Review of the Mechanical and Tribological Behavior of Cold Spray Metal Matrix Composites. *J. Therm. Spray Technol.* **2020**, *29*, 1565–1608. [[CrossRef](#)]
9. Woo, D.J.; Heer, F.C.; Brewer, L.N.; Hooper, J.P.; Osswald, S. Synthesis of Nanodiamond-Reinforced Aluminum Metal Matrix Composites Using Cold-Spray Deposition. *Carbon* **2015**, *86*, 15–25. [[CrossRef](#)]
10. Shao, C.; Zhao, S.; Wang, X.; Zhu, Y.; Zhang, Z.; Ritchie, R.O. Architecture of High-Strength Aluminum–Matrix Composites Processed by a Novel Microcasting Technique. *NPG Asia Mater.* **2019**, *11*, 69. [[CrossRef](#)]
11. Vogt, R.; Zhang, Z.; Topping, T.; Lavernia, E.; Schoenung, J. Cryomilled Aluminum Alloy and Boron Carbide Nano-Composite Plate. *J. Mater. Process. Technol.* **2009**, *209*, 5046–5053. [[CrossRef](#)]
12. Rawal, S.P. Metal-Matrix Composites for Space Applications. *JOM* **2001**, *53*, 14–17. [[CrossRef](#)]
13. Bodunrin, M.O.; Alaneme, K.K.; Chown, L.H. Aluminium Matrix Hybrid Composites: A Review of Reinforcement Philosophies; Mechanical, Corrosion and Tribological Characteristics. *J. Mater. Res. Technol.* **2015**, *4*, 434–445. [[CrossRef](#)]
14. Bakshi, S.R.; Wang, D.; Price, T.; Zhang, D.; Keshri, A.K.; Chen, Y.; McCartney, D.G.; Shipway, P.H.; Agarwal, A. Microstructure and Wear Properties of Aluminum/Aluminum–Silicon Composite Coatings Prepared by Cold Spraying. *Surf. Coat. Technol.* **2009**, *204*, 503–510. [[CrossRef](#)]
15. Shockley, J.; Strauss, H.; Chromik, R.; Brodusch, N.; Gauvin, R.; Irissou, E.; Legoux, J.-G. In Situ Tribometry of Cold-Sprayed Al–Al<sub>2</sub>O<sub>3</sub> Composite Coatings. *Surf. Coat. Technol.* **2013**, *215*, 350–356. [[CrossRef](#)]
16. Xie, X.; Yin, S.; Raelison, R.; Chen, C.; Verdy, C.; Li, W.; Ji, G.; Ren, Z.; Liao, H. Al Matrix Composites Fabricated by Solid-State Cold Spray Deposition: A Critical Review. *J. Mater. Sci. Technol.* **2021**, *86*, 20–55. [[CrossRef](#)]

17. Huang, R.; Sone, M.; Ma, W.; Fukanuma, H. The Effects of Heat Treatment on the Mechanical Properties of Cold-Sprayed Coatings. *Surf. Coat. Technol.* **2015**, *261*, 278–288. [[CrossRef](#)]
18. Rokni, M.; Widener, C.; Champagne, V.; Crawford, G. Microstructure and Mechanical Properties of Cold Sprayed 7075 Deposition during Non-Isothermal Annealing. *Surf. Coat. Technol.* **2015**, *276*, 305–315. [[CrossRef](#)]
19. Rokni, M.; Widener, C.; Ozdemir, O.; Crawford, G. Microstructure and Mechanical Properties of Cold Sprayed 6061 Al in As-Sprayed and Heat Treated Condition. *Surf. Coat. Technol.* **2017**, *309*, 641–650. [[CrossRef](#)]
20. Loganathan, A.; Rengifo, S.; Hernandez, A.F.; Zhang, C.; Agarwal, A. Effect of Nanodiamond Reinforcement and Heat-Treatment on Microstructure, Mechanical and Tribological Properties of Cold Sprayed Aluminum Coating. *Surf. Coat. Technol.* **2021**, *412*, 127037. [[CrossRef](#)]
21. Norrell, T.; Ferguson, G.; Ansell, T.; Saladin, T.; Nardi, A.; Nieto, A. Synthesis and Corrosion Behavior of Cold Sprayed Dual Nanoparticle Reinforced Al Coatings. *Surf. Coat. Technol.* **2020**, *401*, 126280. [[CrossRef](#)]
22. Oliver, W.C.; Pharr, G.M. An Improved Technique for Determining Hardness and Elastic Modulus Using Load and Displacement Sensing Indentation Experiments. *J. Mater. Res.* **1992**, *7*, 1564–1583. [[CrossRef](#)]
23. Page, T.F.; Hainsworth, S.V. Using Nanoindentation Techniques for the Characterization of Coated Systems: A Critique. *Surf. Coat. Technol.* **1993**, *61*, 201–208. [[CrossRef](#)]
24. Bull, S. Nanoindentation of Coatings. *J. Phys. D Appl. Phys.* **2005**, *38*, R393. [[CrossRef](#)]
25. Hall, A.C.; Cook, D.J.; Neiser, R.A.; Roemer, T.J.; Hirschfeld, D.A. The Effect of a Simple Annealing Heat Treatment on the Mechanical Properties of Cold-Sprayed Aluminum. *J. Therm. Spray Technol.* **2006**, *15*, 233–238. [[CrossRef](#)]
26. Grubbs, F.E. Sample Criteria for Testing Outlying Observations. *Ann. Math. Stat.* **1950**, *1*, 27–58. [[CrossRef](#)]
27. Grubbs, F.E. Procedures for Detecting Outlying Observations in Samples. *Technometrics* **1969**, *11*, 1–21. [[CrossRef](#)]
28. Paul, T.; Zhang, C.; Denis, N.; Boesl, B.; Agarwal, A. Role of Ultrasonic Treatment on Microstructure, Mechanical and Tribological Behavior of 2D Boron Nitride Reinforced Aluminum Composites. *Mater. Sci. Eng. A* **2021**, *809*, 140970. [[CrossRef](#)]

**Disclaimer/Publisher's Note:** The statements, opinions and data contained in all publications are solely those of the individual author(s) and contributor(s) and not of MDPI and/or the editor(s). MDPI and/or the editor(s) disclaim responsibility for any injury to people or property resulting from any ideas, methods, instructions or products referred to in the content.